Organic & Biomolecular Chemistry

ROYAL SOCIETY OF CHEMISTRY

PAPER

View Article Online
View Journal | View Issue

Check for updates

Cite this: *Org. Biomol. Chem.*, 2024, **22**, 1800

Dehydration of alcohols catalyzed by copper(II) sulfate: type II dyotropic reactions and stepwise mechanisms†

Jorge Sánchez-Quesada, [a] Carlos López-Cruz, [a] Abel de Cózar, [b,c,d] Ana Arrieta, [b] Iosune Arrastia [b,c] and Fernando P. Cossío *[b,c]

Dehydration of alcohols in the presence of copper(II) sulfate has been analyzed computationally. Density functional theory (DFT) calculations on selected alcohols indicate that this reaction can take place *via* two possible mechanisms: (a) concerted – although asynchronous – type II dyotropic reactions, or (b) stepwise E1-like processes, in which cleavage of the C–O bond occurs in the first step, followed by *syn* proton elimination. Our calculations show the relationship between the initial alcohol structure and the preferred mechanism, which is a type II dyotropic reaction for primary alcohols, whereas a stepwise process is the favored one when stable carbocation intermediates are energetically accessible. The dehydration of dehydrolinalool (2,7-dimethyl-6-en-1-yn-3-ol, DHL) to yield different alkenes of interest in the fragrance industry is discussed as a case study of its regiochemistry.

Received 15th December 2023,
Accepted 31st January 2024

DOI: 10.1039/d3ob02052e

rsc.li/obc

Open Access Article. Published on 31 January 2024. Downloaded on 2/13/2026 9:36:17 AM.
This article is licensed under a Creative Commons Attribution 3.0 Unported Licence.

1. Introduction

Alkenes are essential compounds in the chemical industry due to their versatility associated with the existence of the reactive carbon–carbon double bond. In fact, they are starting materials or key intermediates in the synthetic routes of many valuable compounds such as drugs, pesticides, plastics and fragrances. Therefore, knowledge of the mechanism of alkene synthesis is very important for the development and optimization of industrial processes.

Among all the alkene synthetic methods reported in the literature, one of the most used protocols involves the dehydration of readily accessible alcohols by heating in the presence of an acid catalyst. This method is denoted as hydro-hydroxy-β-elimination and it is usually carried out using concentrated sulfuric or phosphoric acid.[1]

According to the accepted mechanism of the hydro-hydroxy-β-elimination of alcohols in an acidic environment,[2] the first step corresponds to the protonation of a hydroxy moiety to generate an alkyloxonium cation intermediate, which is a better nucleofuge than a hydroxyl anion. This rate-limiting step releases water and the resulting carbenium ion deprotonates to generate a C=C double bond. Generally, three different mechanisms are considered depending on whether water loss and deprotonation occur simultaneously (E2) or sequentially (E1 if the first step is water release or E1cB if deprotonation occurs initially).[3]

The E1 mechanism involves the formation of a carbocation in the rate-determining step; therefore, it is prone to different migration processes. Noteworthily, if more than one β-hydrogen is available, the most substituted *trans*-alkene is preferentially produced, in line with Saytzeff's rule (). The general preference order of the substitution degree of the final alkene is tertiary > secondary > primary, which correlates with the relative stabilities of the corresponding carbenium intermediates.

Another protocol reported in the literature is the pyrolytic *syn*-elimination of alcohol derivatives. These latter compounds include esters, xanthates (Chugaev's elimination), amine *N*-oxides (Cope's elimination) or sulfamate ester intermediates (the Burgess dehydration). In these cases, the accepted mechanism involves a cyclic transition state where the two groups (a hydroxyl derivative or an *N*-oxide and a β-hydrogen atom) leave in a concerted (but not necessarily synchronous) manner. As in the previous cases, this 1,2-elimination reaction usually follows Saytzeff's rule.

[a]*International Flavours & Fragrances IFF Inc., Avda. Felipe Klein 2, Benicarló 12580, Castellón, Spain*
[b]*Department of Organic Chemistry I, Facultad de Química, Kimika Fakultatea, Universidad del País Vasco, Euskal Herriko Unibertsitatea (UPV/EHU), Manuel de Lardizabal 3, 20018 San Sebastián, Donostia, Spain. E-mail: fp.cossio@ehu.es*
[c]*Donostia International Physics Center (DIPC), Manuel de Lardizabal 4, 20018 Donostia, San Sebastián, Spain*
[d]*IKERBASQUE, Basque Foundation for Science, Plaza Euskadi 5, 48009 Bilbao, Spain*

† Electronic supplementary information (ESI) available. See DOI: https://doi.org/10.1039/d3ob02052e

This journal is © The Royal Society of Chemistry 2024

Open Access Article. Published on 31 January 2024. Downloaded on 2/13/2026 9:36:17 AM.
This article is licensed under a Creative Commons Attribution 3.0 Unported Licence.

A related mechanism that can yield alkenes **2** from alcohols **1** *via* a catalytic type II dyotropic reaction[4–7] can be envisaged. This reaction consists of a double group transfer (in our case, a hydrogen atom and a hydroxy group) from the alcohol to a bifunctional catalyst that can be regenerated *via* a subsequent dehydration (Scheme 1). Given the nature of this catalyst, an alternative E2 mechanism *via* an antiperiplanar transition structure would be of higher energy. This reaction would be *syn*-1,2-elimination that does not require the formation of an alcohol derivative. This concerted reaction can evolve in a continuous manner by losing synchronicity towards a stepwise E1-like dehydroxy-dehydro elimination reaction, in which a carbenium hydroxy ionic pair is the key intermediate (Scheme 1).

The catalytic dehydration of alcohols in the presence of $CuSO_4$, both in solution[8–12] and adsorbed on silica gel,[13,14] to yield alkenes is a useful method for the chemical synthesis of alkenes *via* a formal 1,2-elimination reaction that can be envisaged within the conceptual framework presented in Scheme 1. This procedure requires relatively high temperatures and avoids undesired rearrangements or the preparation of more reactive ester intermediates. Despite its practical and conceptual interest, this reaction has been scarcely described in the literature and no details about the nature of its mechanism have been reported so far.

In 1980, Hoffman and co-workers[10] published an outline of the species involved in the catalytic activity of this reaction. The authors explored the reactivity of several alcohols and reported the tertiary ≈ benzylic > allylic > secondary reactivity trend. In view of these results, the authors hypothesized that carbenium ion formation is the key step of the reaction. This proposal was supported by the observation that Saytzeff-type regiochemistry is favoured and *trans*-olefins are obtained as major stereoisomers. Another remarkable experimental finding is that the addition of small amounts of pyridine to the reaction mixture inhibits the catalytic activity. However, no explanation about the role of copper in the dehydration reaction was provided. Within this context and taking into account our previous studies on dyotropic reactions,[15–22] we considered the occurrence of a type II dyotropic reaction in this catalytic dehydration reaction as a starting hypothesis. Of course, depending upon the evolution of synchronicity in these reactions induced by different substituents, a transition from concerted to stepwise mechanisms could be envisaged.

Based on these antecedents and our starting hypothesis, in this paper, we report our results on the mechanism of the dehydration reaction of alcohols catalyzed by monomeric $CuSO_4$. We selected several significant examples in order to gain a better understanding of the regio- and stereochemistry of this reaction. In addition, a relevant case of industrial interest was also studied.

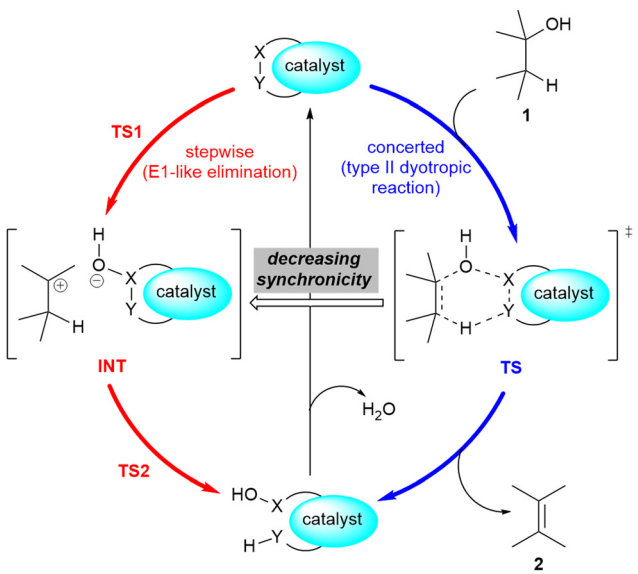

Scheme 1 Possible 1,2-dehydration of alcohols **1** *via* type II dyotropic and E1-like elimination reactions. The possible substituents in alcohol **1** and alkene **2** are not specified.

2. Computational details

Optimization of geometries and thermochemical calculations were carried out using the Minnesota M06[23,24] meta-GGA functional. Energies were computed by means of the Tao–Perdew–Staroverov–Scuseria TPSS[25,26] correlation-exchange functional in order to get more accurate energy barriers. In calculations with this latter functional, Grimme D3 with the Becke–Jones damping potential[27] (D3BJ) was included to improve the description of dispersion energies. All the calculations were carried out using the Gaussian 16[28] suite of programs. Solvent effects were estimated by the polarization continuum model (PCM) method using the self-consistent reaction field (SCRF) approach.[29] All SCRF-PCM calculations were performed using methanol (ε = 32.613) as the model solvent. For the calculation of Gibbs energies, standard conditions at different temperatures (298.15 or 423.15 K, 1 M) were assumed. The standard 6-31G(d,p) basis set was used for C, O, S and H atoms. The Hay–Wadt[30] small core effective potential (ECP) including a double-ξ valence basis set (invoked by the LanL2dz keyword) was used for Cu atoms. Gibbs activation barriers were computed within the DFT[31] framework at the M06(PCM)/6-31G(d,p)&LanL2dz level of theory using TPSS-D3BJ(PCM)/6-31G(d)&LanL2dz//M06(PCM)/6-31G(d,p)&LanL2dz total energies.

The unrestricted spin approximation (UM06) was used because of the formal doublet character of Cu(II), with a correction of spin contamination to keep $\langle S^2 \rangle \approx 0.75$ a.u.

All the stationary points were characterized by harmonic vibrational analysis.[32] Local minima showed positive definite Hessians. Fully optimized transition structures (TSs) showed one and only one imaginary frequency associated with nuclear motion along the chemical transformation under study. Reaction paths were checked using Intrinsic Reaction Coordinate (IRC) calculations.[33,34]

Wiberg bond indexes and Natural Bond Orbital atomic charges were computed within the NBO[35] method

Open Access Article. Published on 31 January 2024. Downloaded on 2/13/2026 9:36:17 AM.
This article is licensed under a Creative Commons Attribution 3.0 Unported Licence.

implemented in Gaussian16. NBO charges on carbon atoms were computed including the charge of hydrogen atoms attached to them. Bond indices[36] B_{AB} between atoms A and B in the NBO basis were computed according to the Wiberg definition:

$$B_{AB} = \sum_{\mu \in A} \sum_{\nu \in B} {P_{\mu\nu}}^2 \quad (1)$$

where $P_{\mu\nu}$ denotes the elements of the density matrix centered on atoms A and B.

Synchronicites[37,38] Sy were computed as defined in eqn (2):

$$\mathrm{Sy} = 1 - \frac{1}{2n-2} \sum_{i=1}^{n} \frac{|\delta B_i - \delta B_{av}|}{\delta B_{av}} \quad (2)$$

in which δB_i is the variation of the bond index B_i from the reactants R to the transition structure TS with respect to the product P, according to the following expression:

$$\delta B_i = \frac{B_i^{TS} - B_i^{R}}{B_i^{P} - B_i^{R}} \quad (3)$$

In eqn (2), δB_{av} is the average value of δB_i for the n chemical bonds being modified along the reaction coordinate, as indicated in eqn (4):

$$\delta B_{av} = n^{-1} \sum_{i=1}^{n} \delta B_i \quad (4)$$

Eqn (2)–(4) provide an intuitive estimate of the synchronicity of the reaction, since for a perfectly synchronous process, $\delta B_i = \delta B_{av}$ for any i = 1, 2..., n and therefore Sy = 1. According to the reaction mechanisms considered in the dehydration reaction catalysed by $CuSO_4$, we considered n = 6 in eqn (2)–(4), as indicated in Scheme 2A, since the remaining bond orders did not vary significantly along the reaction coordinate.

Selectivities were computed using the previously computed Gibbs free activation energies by means of the Eyring equations for the respective elementary steps:

$$k_i = \frac{k_B T}{h} \exp\left(-\frac{\Delta G_a^i}{RT}\right) \quad (5)$$

where k_i and ΔG_a^i are the kinetic constant and the Gibbs activation energy of the step denoted as i.

Given the complex kinetic profiles (*vide infra*) of the dehydration reactions studied, both the Curtin–Hammett kinetics,[39,40] and numerical integration[41] of the respective differential equations were performed, normalizing the concentrations of the different elimination products to 100.

3. Results and discussion

General considerations

In view of the above-mentioned precedents, two possible mechanisms for the dehydration of alcohols in the presence of copper(II) sulfate were envisaged (Scheme 2). In order to obtain a computationally accessible structure, an isolated unit of $CuSO_4$ was considered. In our calculations, we added an additional explicit molecule of alcohol in order to complete the tetra-coordinated environment of the copper(II) centre,[42] thus avoiding spurious interactions between the copper atom and C–H or C=C double bonds. Since this additional alcohol molecule does not participate in the reaction coordinate, we selected methanol (R = Me in Scheme 2) as the model alcohol. The introduction of explicit additional solvent molecules indirectly attached to the Cu atom did not significantly affect the geometry of the stationary points and increased the computed activation barriers (see the ESI†). Therefore, in successive calculations we considered only one explicit molecule of

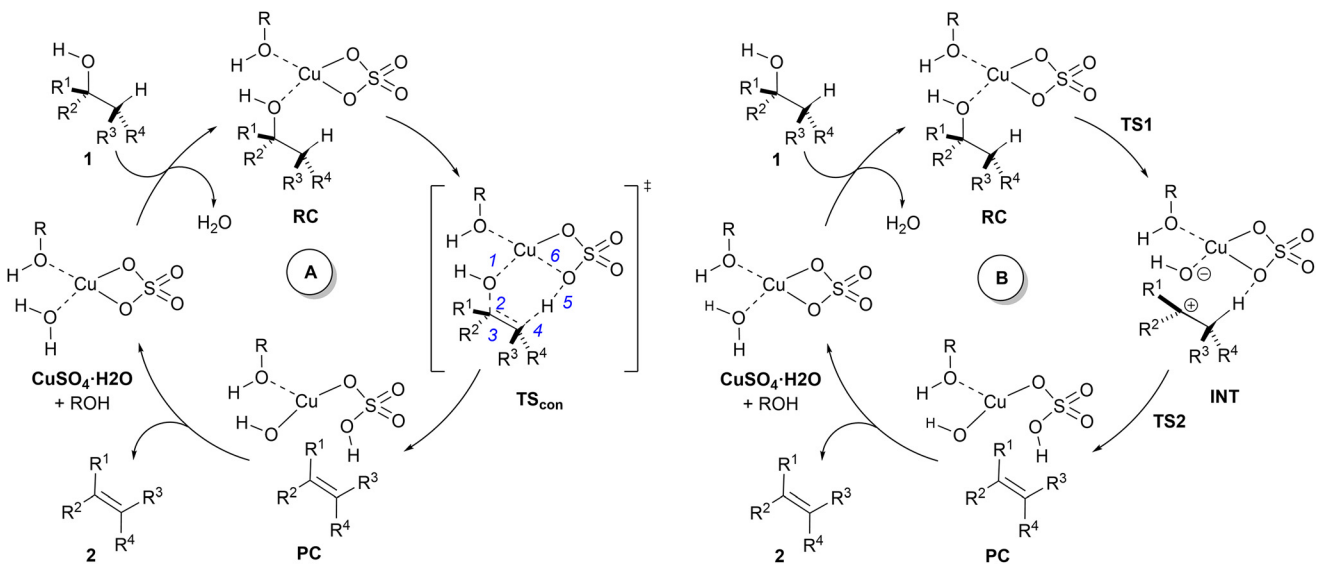

Scheme 2 Proposed mechanism for the dehydration reaction of alcohols catalysed by $CuSO_4$. (A) Concerted type II dyotropic reaction; (B) stepwise E1-like dehydroxy-dehydro elimination. The bonds considered for the calculation of synchronicities (Sy) are indicated for saddle point TS_{con}.

This journal is © The Royal Society of Chemistry 2024

Open Access Article. Published on 31 January 2024. Downloaded on 2/13/2026 9:36:17 AM.
This article is licensed under a Creative Commons Attribution 3.0 Unported Licence.

solvent and tackled the bulk medium by means of the continuum dielectric model. Both mechanisms start with a reactive complex **RC**, in which two equivalents of alcohol **1** interact with $CuSO_4$.

The mechanism denoted as A in Scheme 2 corresponds to the application of the present process of the general type II dyotropic reaction mechanism depicted in Scheme 1. According to this mechanism, the reaction would be concerted with a sole transition structure, denoted as $\mathbf{TS_{con}}$, which connects the reactive complex **RC** with product-like complex **PC**. The copper moiety of this latter complex would evolve towards the formation of the corresponding monohydrate complex, with the concomitant release of alkene **2**. In subsequent catalytic cycles, the Cu(II) centre could coordinate to one or two molecules of alcohol, depending upon the release of one equivalent of water, which should not affect the nature of the mechanism.

Another possible mechanism, denoted as B in Scheme 2, could consist of a stepwise process in which the complete asynchronicity of mechanism A results in the formation of an ionic pair denoted as **INT**. This mechanism requires two transition structures, denoted as **TS1** and **TS2** in Scheme 2. In the first one, the hydroxy group of the starting alcohol **1** is transferred to the metallic centre, thus leaving a carbocationic centre at the former alcohol moiety. The second saddle point **TS2** involves the cleavage of the C–H bond contiguous to the cationic centre to yield complex **PC**, similar to that postulated for mechanism A. In principle, a continuous transition between mechanisms A and B can be expected, depending upon the asynchronicity associated with the saddle point $\mathbf{TS_{con}}$ (mechanism A) and the stability of the carbonium part of ionic pair **INT** (mechanism B).

Computational elucidation of the different mechanisms can be determined by numerical integration of the kinetic equations obtained using the kinetic constants associated with the respective elementary steps as indicated in eqn (5). Assuming a downhill and irreversible evolution of product complexes **PC** to alkenes **2**, the reaction rates can be approximated as

$$\frac{\mathrm{d}[\mathrm{PC}]_{\mathrm{dyo}}}{\mathrm{d}t} = k^{\mathrm{dyo}}[\mathrm{RC}] \tag{6}$$

for the dyotropic mechanism. Within the same kinetic framework, in the case of the stepwise E1-like elimination, the rate associated with the irreversible formation of alkenes **2** is properly described by eqn (7):

$$\frac{\mathrm{d}[\mathrm{PC}]_{\mathrm{stp}}}{\mathrm{d}t} = k^{\mathrm{stp}}[\mathrm{INT}] \tag{7}$$

In both cases, the evolution of the starting reaction complexes corresponding to the different mechanisms is described by the kinetics of matrix Y that includes the reaction intermediates and reactive complexes:

$$-\frac{\mathrm{d}Y}{\mathrm{d}t} = KY \tag{8}$$

In eqn (8), matrix K contains the appropriate kinetic constants, calculated by means of eqn (5).

The concentration $[\mathrm{P_i}]$ of product P_i with respect to the total ensemble of products was calculated according to eqn (9):

$$100\frac{[P_i(t)]}{\sum_j [P_j(t)]} = \%[P_i(t)] \tag{9}$$

We carried out our computational study by analyzing a set of alcohols with different degrees of substitution, which are gathered in Scheme 3. Ethanol (**1a**), cyclohexanol (**1b**), 1-phenylethan-1-ol (**1c**) and 2-phenylpropan-2-ol (**1d**) do not pose regiochemical issues, since these alcohols can only yield ethene (**2a**), cyclohexene (**2b**), styrene (**2c**) and 1-methyl styrene (**2d**) as unsubstituted, monosubstituted and disubstituted alkenes. Instead, 2-hexanol (**1e**) can yield two regioisomers that can be classified as Saytzeff **2e(Sz)** and anti-Saytzeff **2e(aS)** trisubstituted and disubstituted alkenes, respectively. Finally, the dehydration of dehydrolinalool (**1f**) was studied. This alcohol is of great interest in the flavour and fragrance industry[43] and can yield two Saytzeff stereoisomers, denoted as **(*E*)-**

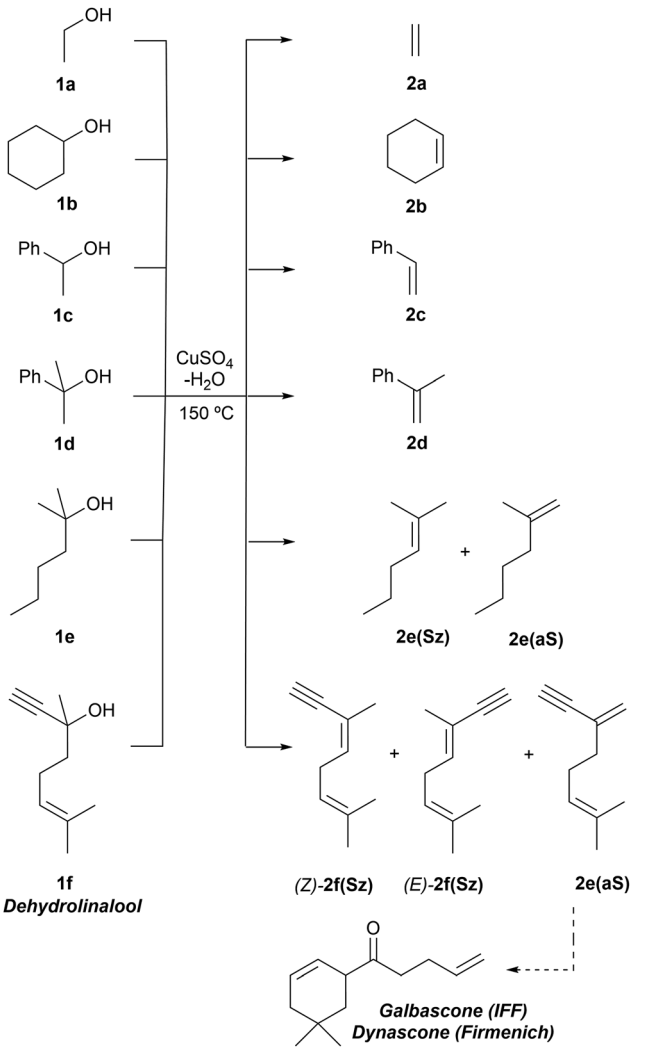

Scheme 3 Dehydration reactions studied in this work.

Open Access Article. Published on 31 January 2024. Downloaded on 2/13/2026 9:36:17 AM.
This article is licensed under a Creative Commons Attribution 3.0 Unported Licence.

2f(Sz) and **(*Z*)-2f(Sz)** in Scheme 3, and one anti-Saytzeff alkene, denoted as **2f(aS)**. This latter compound is a key intermediate in the synthesis of Galbascone or Dynascone (1-(5,5-dimethyl-cyclohexen-1-yl)pent-4-en-1-one), a synthetic fragrance of great industrial interest.[44] The computed Gibbs free energy reaction profiles and the main geometrical features of the transition structures for the dehydration of **1a–f** were collected and are shown in Fig. 1–10. Free energies were computed at 25 °C (298.15 K) and 150 °C (423.15 K), since the reported experimental studies were conducted at temperatures ranging from 120 °C to 150 °C.

Dehydration of ethanol

The parent reaction **1a** → **2a** was computed first. The corresponding reaction profile is shown in Fig. 1. According to our results, copper(II) sulfate forms a stable complex **RCa** with **1a** due to the initial interaction between the oxygen atom of the alcohol and the metallic centre. From this reactive complex, alkene **2a** is formed *via* $\mathbf{TS_{con}a}$ in a single step, with an activation barrier of *ca.* 35 kcal mol^{-1} to generate the product complex **PCa** in which the double C=C bond is generated with the concomitant breaking of one of the Cu–O bonds of Cu(II) sulphate. This high-energy barrier is in full agreement with the fact that $CuSO_4$ is not used as a catalyst in the industrial dehydration reaction of ethylene[45] and with the poor reactivity

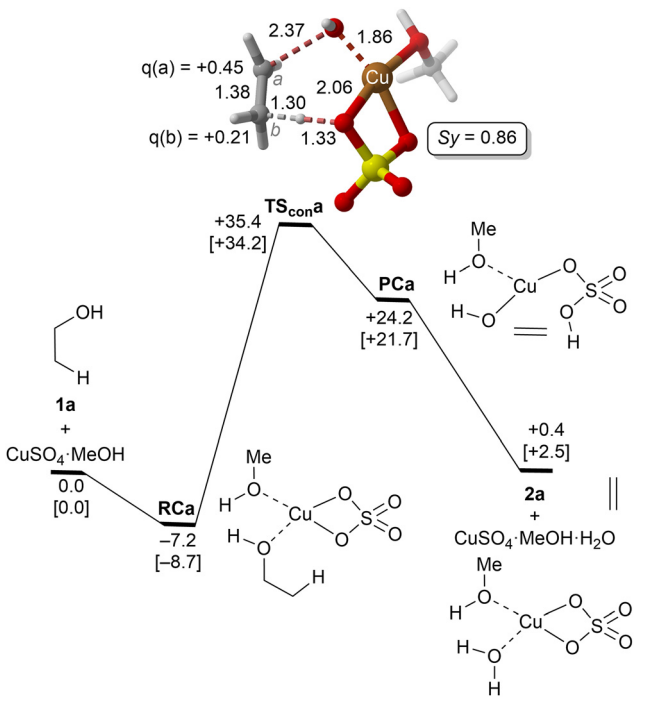

Fig. 1 Reaction profile and the main geometrical features of the transition structure associated with the elimination reaction of alcohol **1a** catalyzed by $CuSO_4$ computed at the UTPSS-D3BJ/(PCM)/6-31G(d,p)&LanL2dz//UM06(PCM)/6-31G(d,p)&LanL2dz level of theory. Relative Gibbs energies, in kcal mol^{-1}, were computed at 298.15 K and 423.15 K (values between brackets). Synchronicities were calculated using eqn 2. Distances are in Å. Relevant NBO charges are also included.

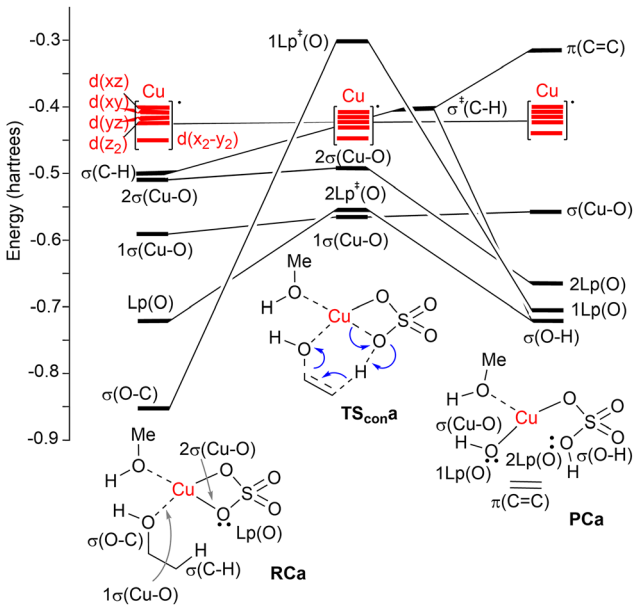

Fig. 2 Correlation NBO diagram for the transformation of reactive complex **RCa** into **PCa** *via* $\mathbf{TS_{con}a}$. The blue curved arrows show the electronic motion along the reaction coordinate.

of primary alcohols. Geometric inspection of $\mathbf{TS_{con}a}$ shows that it corresponds to a slightly asynchronous type II dyotropic reaction (Sy = 0.86), in which the reagent C–O bond breaking process is more developed than the cleavage of the C–H bond. This is reflected in the long C–O critical bond distance in $\mathbf{TS_{con}a}$ and the higher positive NBO charge computed for C(a), which shows a partial primary carbocation character. Noteworthily, transformation of the product complex into hydrated copper(II) sulfate is required to make the reaction slightly exergonic with respect to the isolated reagents. Once hydrated copper(II) sulfate is formed, reactive complex **RCa** is regenerated *via* an exergonic water–alcohol exchange, thus closing the catalytic cycle (see the ESI†).

Alternative reaction mechanisms, in which copper(II) complexes act as Brønsted acids, *i.e.*, ethanol (**1a**) protonation as the initial step of the elimination process, were also evaluated. Our results show that this latter process is endergonic (see the ESI†). Therefore, this mechanistic hypothesis was not further investigated.

A correlation diagram of the localized NBOs of **RCa**, $\mathbf{TS_{con}a}$ and **PCa** permitted us to analyze this parent reaction, thus gaining a better understanding of the nature of the electronic changes along the reaction coordinate associated with this type II dyotropic transfer reaction. Firstly, we observed that the d-AOs of Cu(II) are not involved in the reaction, since they remain essentially unaffected. Secondly, it was concluded that the C(b)–H bond is transformed into a σ(O–H) localized MO and the π(C=C) double bond, whereas one σ(CuO) localized MO becomes a lone pair centered at one oxygen atom. Instead, the initial σ(C–O) bond evolves towards a localized lone pair centered on the oxygen of the new hydroxyl group bound to

This journal is © The Royal Society of Chemistry 2024

Open Access Article. Published on 31 January 2024. Downloaded on 2/13/2026 9:36:17 AM.
This article is licensed under a Creative Commons Attribution 3.0 Unported Licence.

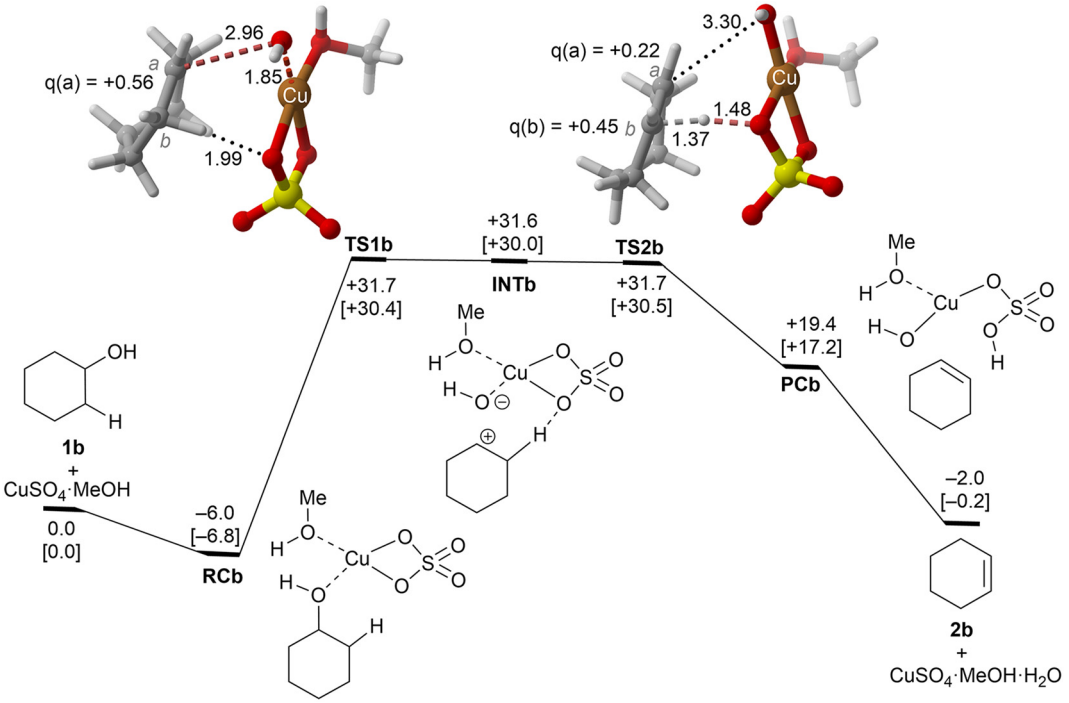

Fig. 3 Reaction profile and the main geometrical features of the transition structure associated with the elimination reaction of alcohol **1b** catalyzed by $CuSO_4$. See the caption of Fig. 1 for more details.

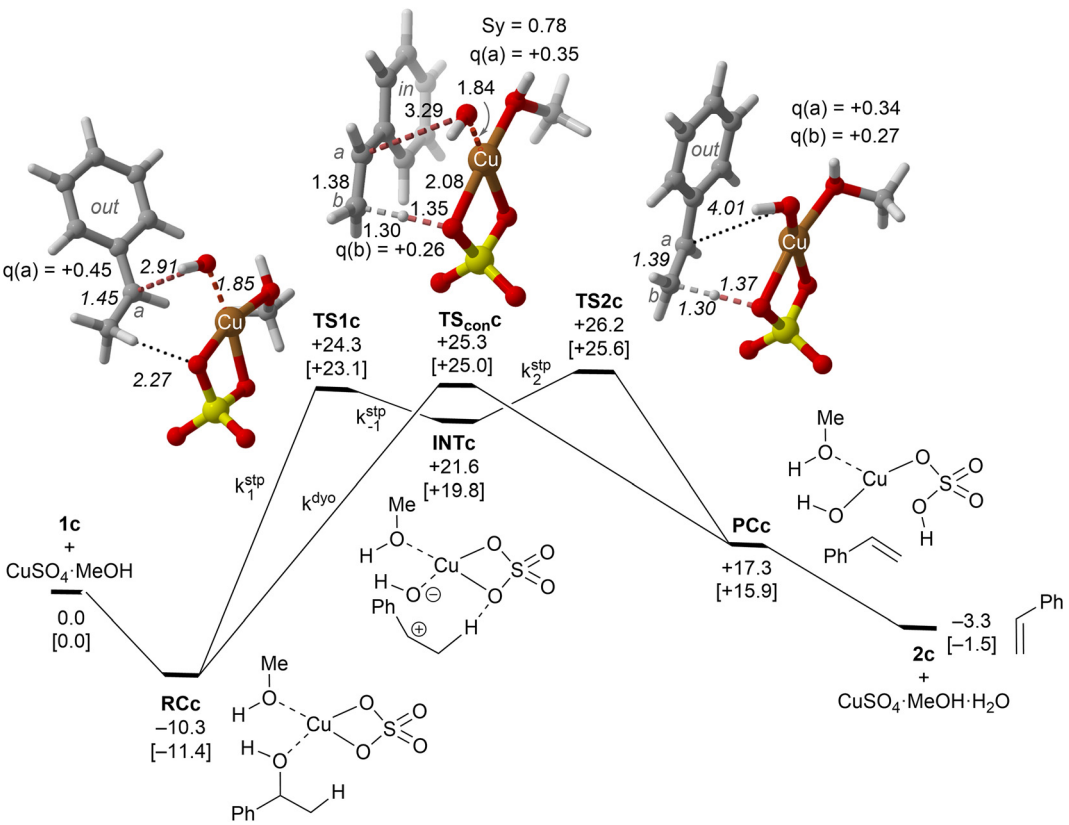

Fig. 4 Reaction profile and the main geometrical features of the transition structure associated with the elimination reaction of alcohol **1c** catalyzed by $CuSO_4$. The kinetic constants associated with each elementary step are also indicated. See the caption of Fig. 1 for more details.

Open Access Article. Published on 31 January 2024. Downloaded on 2/13/2026 9:36:17 AM.
This article is licensed under a Creative Commons Attribution 3.0 Unported Licence.

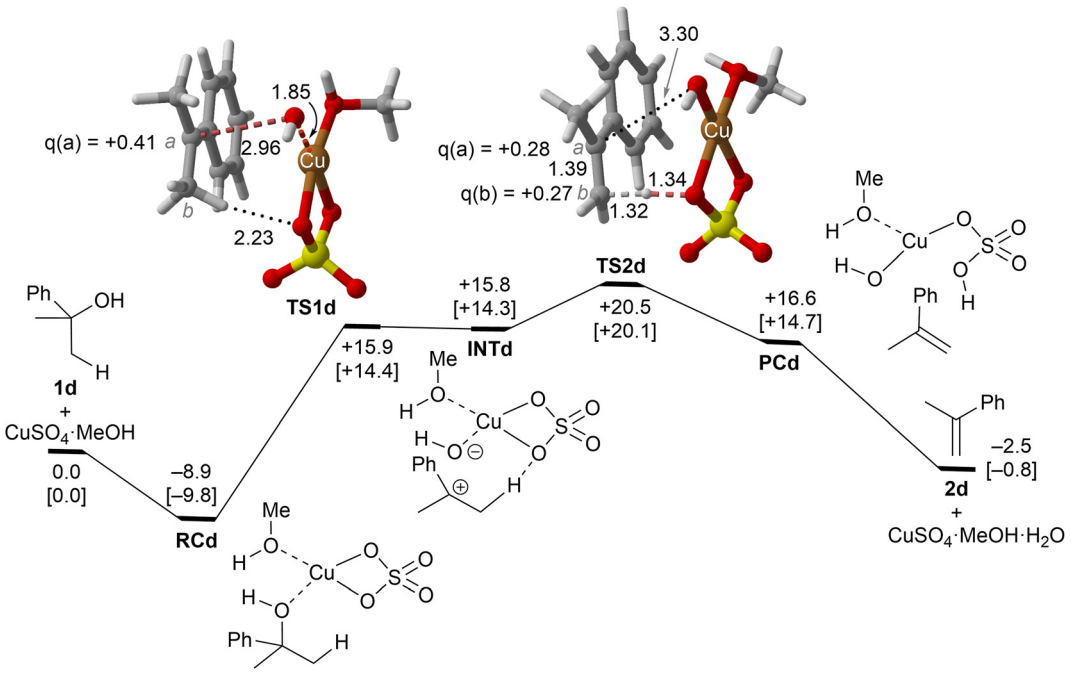

Fig. 5 Reaction profile and the main geometrical features of the transition structure associated with the elimination reaction of alcohol **1d** catalyzed by $CuSO_4$. See the caption of Fig. 1 for more details.

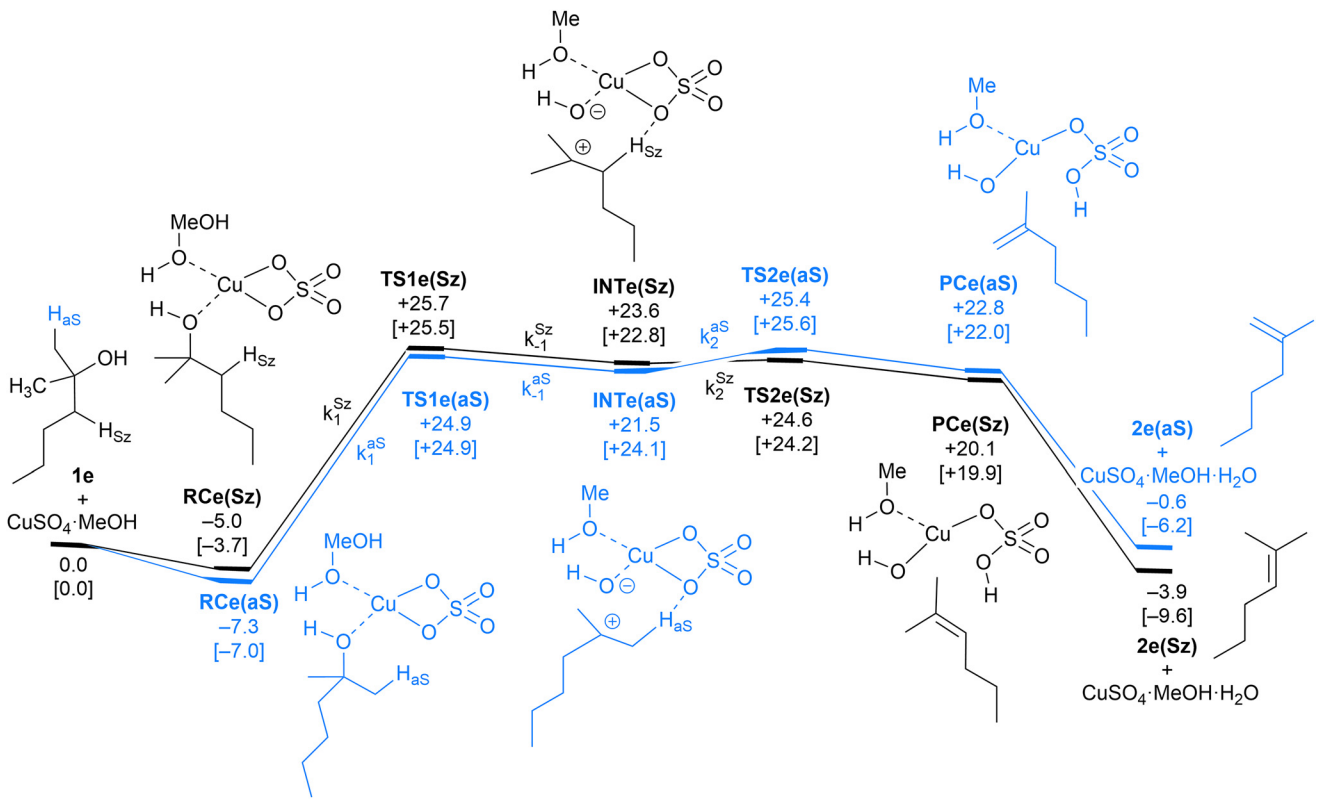

Fig. 6 Computed Saytzeff (Sz) and anti-Saytzeff (aS) reaction profiles associated with possible elimination reactions of hexan-2-ol (**1e**) catalyzed by $CuSO_4$. See the caption of Fig. 1 for further details. Selected kinetic constants for elementary steps are also given (see eqn (12)–(15)).

This journal is © The Royal Society of Chemistry 2024

Open Access Article. Published on 31 January 2024. Downloaded on 2/13/2026 9:36:17 AM.
This article is licensed under a Creative Commons Attribution 3.0 Unported Licence.

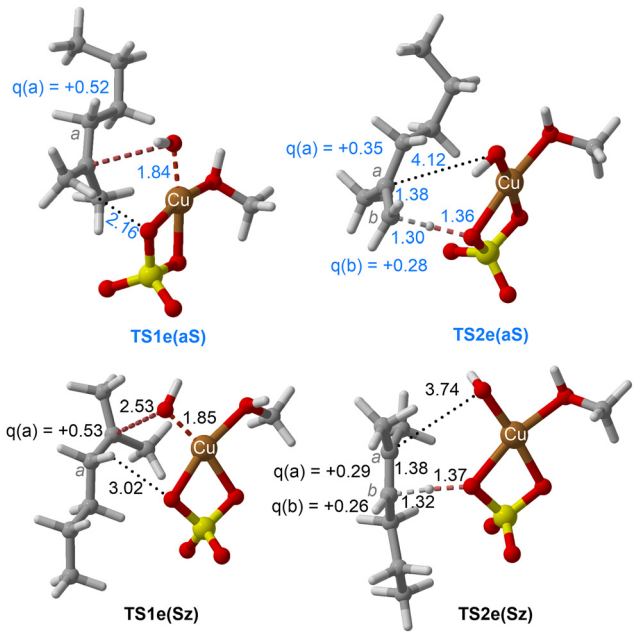

Fig. 7 Chief geometrical features of Saytzeff (Sz) and anti-Saytzeff (aS) transition structures associated with possible elimination reactions of hexan-2-ol (**1e**) catalyzed by $CuSO_4$. See the caption of Fig. 1 for more details.

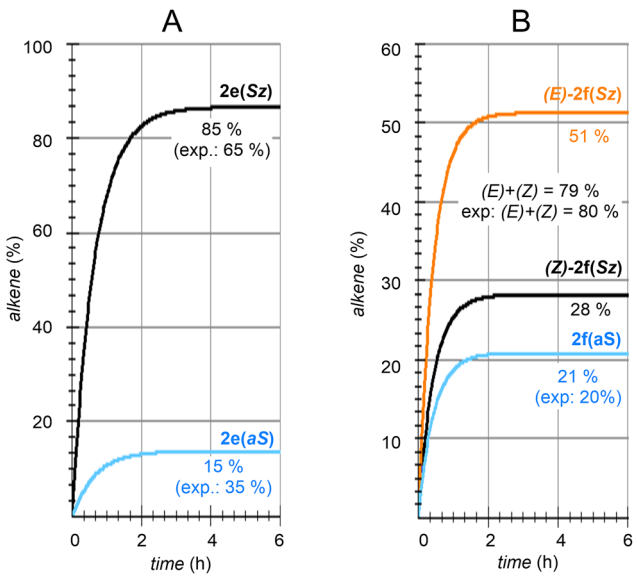

Fig. 8 Numerical simulation of the calculated regio- and stereochemistry associated with the dehydration reaction of hexan-2-ol (**1e**) and dehydrolinalool (**1f**) catalyzed by $CuSO_4$.

copper(II). The whole ensemble of NBOs shows electronic circulation along the cyclic transition structure. This analysis also shows a strong destabilization in $\mathbf{TS_{con}a}$ and the endergonic character of this elementary step, fully compatible with the high activation energy associated with this reaction, which precludes its use in practical transformations. A lesser contribution of the term associated with the highly energetic cleavage of the localized σ(C–H) orbital should result in a stepwise process with a lower activation energy. Likewise, a more substituted carbon atom linked to the hydroxy group would result in a lower NBO σ(C–O) → $Lp^{\ddagger}$(O) transition, associated with a lower activation energy and a stepwise mechanism.

Dehydration of cyclohexanol, 1-phenylethan-1-ol and 2-phenylpropan-2ol

These alcohols were selected because of their different structural and electronic features and lack of regiochemical issues.

In the case of cyclohexanol (**1b**), our calculations show that the dehydration process corresponds to a stepwise mechanism, in which the initial C–O bond breaking process (**TS1b**) leads to the formation of a highly unstable ionic pair **INTb**, and the alcohol moiety is transformed into a secondary carbocation intermediate. Evaluation of the ion pair dissociation energy shows that **INTb** is a stable enough intermediate, whose dissociation energy is of *ca.* 15 kcal mol^{-1} (see the ESI†). Therefore, E1 elimination without the participation of Cu(II) sulphate in the C–H dehydro step was not considered. In this case, the secondary carbenium centre is stable enough to favor the dehydroxy-dehydro stepwise elimination instead of the dyotropic process. Once the development of the positive charge on the carbon atom proceeds, the potential energy surface is almost flat, and **INTb** evolves into cyclohexene through saddle point **TS2b** *via* an essentially barrierless process. Noteworthily, in this latter transition structure, the C(b) charge is higher than the one of C(a) due to the electron density transfer from the C–H breaking bond. The computed activation barrier corresponding to the rate-limiting step is *ca.* 4 kcal mol^{-1} lower than the one computed for ethanol **1a**, a result in line with the reactivity trend described experimentally. In addition, as in the previous case, the transformation of the product complex onto hydrated copper(II) sulfate is also required to make the reaction exergonic.

Our calculations show that the dehydration reaction obtained for 1-phenylethan-1ol (**1c**) is compatible with both mechanisms (Fig. 4). This result was surprising because it is known that benzylic carbocations are more stable than other secondary carbocations (such as **INTb**) due to the charge delocalization (resonance) of the benzylic moiety. Therefore, *a priori*, a stepwise mechanism analogous to cyclohexanol (**1b**) would be expected. However, careful inspection of $\mathbf{TS_{con}c}$ shows the existence of a stabilizing interaction between the inner (denoted as *in* in Fig. 4) phenyl group and the copper(II) atom that favors the existence of the concerted dyotropic transition structure. In $\mathbf{TS_{con}c}$, the breaking of the C–O bond is more developed than that of the C–H one as reflected by the C–O bond distance of 3.29 Å, where the charge on C(a) is also delocalized in the phenyl ring. This concerted saddle point is less synchronous than the parent congener $\mathbf{TS_{con}a}$ (Sy = 0.78, see Fig. 4). However, when the phenyl group is in an outer orientation with respect to the Cu(II) centre, the stabilizing interaction observed in $\mathbf{TS_{con}c}$ is not present and the mechanism turns out to be stepwise (Fig. 4). In this latter case, the

Open Access Article. Published on 31 January 2024. Downloaded on 2/13/2026 9:36:17 AM.
This article is licensed under a Creative Commons Attribution 3.0 Unported Licence.

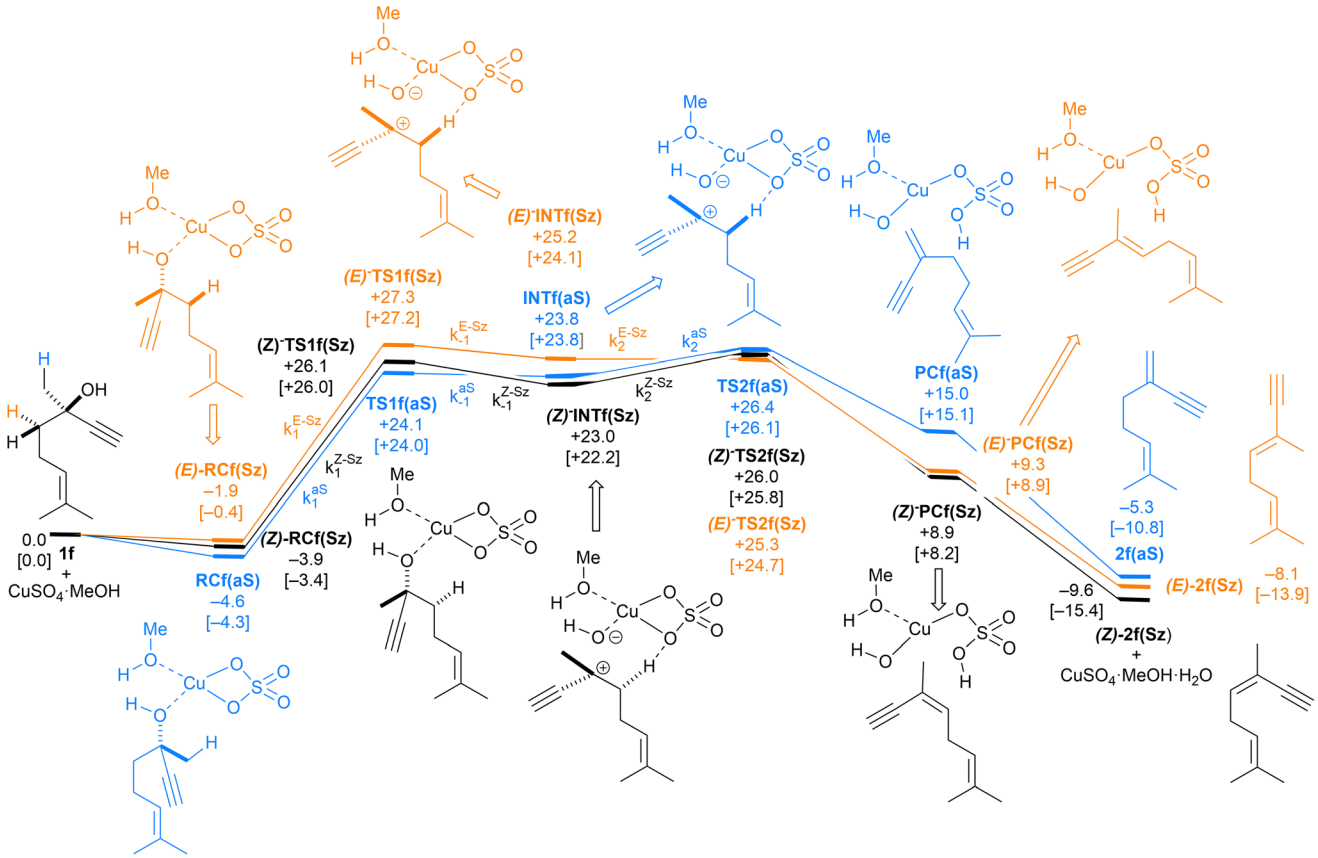

Fig. 9 Computed reaction profile and the main geometrical features of the transition structure associated with all possible elimination reactions of dehydrolinalool (**1f**) catalyzed by $CuSO_4$. See the caption of Fig. 1 for more details.

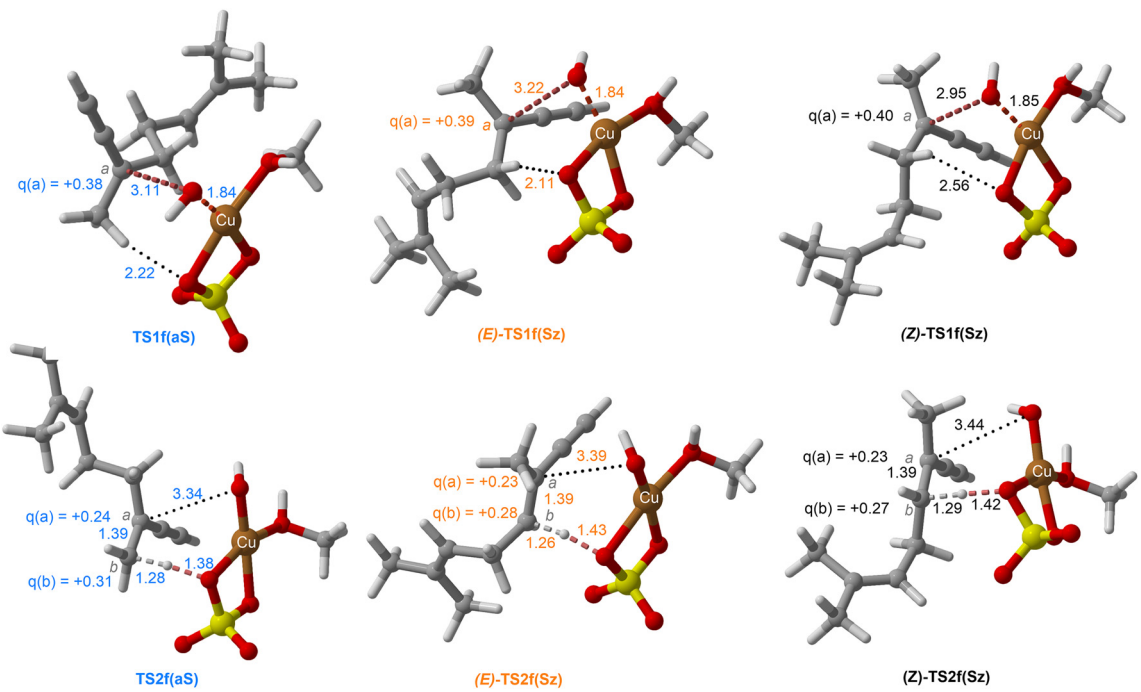

Fig. 10 Chief geometrical features of Saytzeff (Sz) and anti-Saytzeff (aS) transition structures associated with possible elimination reactions of hexan-2-ol (**1e**) catalyzed by $CuSO_4$. See the caption of Fig. 1 for more details.

This journal is © The Royal Society of Chemistry 2024

Open Access Article. Published on 31 January 2024. Downloaded on 2/13/2026 9:36:17 AM. This article is licensed under a Creative Commons Attribution 3.0 Unported Licence.

rate-limiting step takes place *via* **TS1c** and leads to the ionic pair **INTc**. From this intermediate, the product complex **PCc** is formed *via* **TS2c**, with an activation energy of *ca.* 6 kcal mol^{-1} at 150 °C. The energies of $\mathbf{TS_{con}c}$ and **TS1c** are quite similar, with the concerted saddle point being *ca.* 2 kcal mol^{-1} more energetic than its first stepwise congener. However, the stepwise mechanism requires an additional energy barrier to yield alkene **2c**. In order to quantify the relative participation of both mechanisms, we applied eqn (6)–(8), in which the matrix of intermediates Y_c is:

$$Y_c = \begin{pmatrix} [\mathrm{RCc}] \\ [\mathrm{INTc}] \end{pmatrix} \tag{10}$$

and the kinetic constant matrix K_c was defined as

$$K_c = \begin{pmatrix} k^{dyo} + k_1^{stp} & -k_{-1}^{stp} \\ -k_1^{stp} & k_2^{stp} + k_{-1}^{stp} \end{pmatrix} \tag{11}$$

In eqn (11), the kinetic constants are defined in Fig. 4. Using the values obtained from the respective activation energies, we obtained a dyotropic : stepwise ratio of 70 : 30. Therefore, in the **1c** → **2c** dehydration reaction, the type II dyotropic reaction is the major contributor to the two-component mechanism shown in Fig. 4.

Copper(II) sulfate-catalyzed dehydration of 2-phenylpropan-2-ol (**1d**) follows a stepwise mechanism, in which resonance-stabilized carbocation intermediate **INT1d** is formed after the C–O bond breaking step. In the rate-limiting step, the long C–O critical distance of **TS1d** is compatible with the late character of this saddle point, in which the C–O bond breaking process is quite advanced and associated with an activation barrier of 24 kcal mol^{-1} with respect to **RCd**. In addition, the positive charge in C(a) is clearly developed. In contrast to the **1b** case, the activation barrier associated with the second step is not negligible (5–6 kcal mol^{-1}). Remarkably, the energy required for this process is lower than the activation barriers associated with the dehydration of **1a** or **1b** and **1c**, in agreement with the tertiary > secondary > primary alcohol reactivity trend reported experimentally.

Regiochemistry

The dehydration reaction of 2-hexanol (**1e**) offers a more complicated scenario than the above discussed alcohols since two alkenes can be formed: highly substituted (Saytzeff) **2e(Sz)** and less substituted (anti-Saytzeff) **2e(aS)** (Scheme 3). The computed energetic profiles collected in Fig. 6 correspond to a stepwise elimination in both cases, as expected for a tertiary alcohol that would generate a stable carbocation intermediate after the initial transfer of the hydroxyl moiety to the metallic centre. We computed two different reaction profiles associated with the C–O bond breaking process anticipating the structure of the final alkenes through $\mathrm{C–H_{Sz/aS}}\cdots\mathrm{Cu}$ interactions *via* saddle points **TS1e(Sz)** and **TS1e(aS)**. The activation barriers associated with these initial steps are slightly different. However, the carbocations **INTe(Sz)** and **INTe(aS)** are close in energy. Therefore, the selectivity towards Saytzeff or anti-Saytzeff cannot be related directly to this initial step, since the subsequent hydrogen elimination must play a significant role. Evaluation of the NBO charges (Fig. 7) shows more developed charges on **TS2a(aS)** than on **TS2e(Sz)**. The positive charge on C(b) of **TS2e(aS)** indicates a significant character of a highly unstable primary carbocation, which makes the $\mathrm{C–H_{aS}}$ bond breaking more energetic compared to **TS2e(Sz)**, in which the charge is stabilized by the alkyl substituent, thus making a higher barrier for the formation of **2e(aS)**. Based on the obtained reaction profiles, we computed the Saytzeff/anti-Saytzeff ratio of alkenes **2e** assuming their irreversible formation *via* the downhill release of the alkene moiety in product complexes **PCe(Sz)** and **PCe(aS)**, respectively:

$$\mathrm{rate(Saytzeff)} = \frac{\mathrm{d[PCe(Sz)]}}{\mathrm{d}t} = k_2^{Sz}[\mathrm{INTe(Sz)}] \tag{12}$$

$$\mathrm{rate(anti\text{-}Saytzeff)} = \frac{\mathrm{d[PCe(aS)]}}{\mathrm{d}t} = k_2^{aS}[\mathrm{INTe(aS)}] \tag{13}$$

Now, the corresponding matrix Y_e is:

$$Y_e = \begin{pmatrix} [\mathrm{RCe}] \\ [\mathrm{INTe(Sz)}] \\ [\mathrm{INTe(aS)}] \end{pmatrix} \tag{14}$$

in which the reactive complexes are assumed to be in equilibrium. The kinetic constant matrix K_e, whose terms are indicated in Fig. 6, is as follows:

$$K_e = \begin{pmatrix} k_1^{Sz} + k_1^{aS} & -k_{-1}^{Sz} & -k_{-1}^{aS} \\ -k_1^{Sz} & k_{-1}^{Sz} + k_2^{Sz} & 0 \\ -k_1^{aS} & 0 & k_{-1}^{aS} + k_2^{aS} \end{pmatrix} \tag{15}$$

The solution of eqn (8) and (12)–(15) by numerical integration yields the kinetic profiles gathered in Fig. 8A. According to our results, the Saytzeff : anti-Saytzeff ratio is 85 : 15, in qualitative agreement with the experimentally observed 65 : 35 and in line with the observations of Hofmann about the Saytzeff regioselectivity.[10]

All our attempts to locate a transition structure connecting **INTe(Sz)** and **INTe(aS)** met with no success. This result suggests that the potential energy surface is very complex in this region of the reaction coordinate or that both intermediates can equilibrate before the second transition structures **TS2e(Sz)** and **TS2e(aS)** despite the fact that our IRC analysis connected these saddle points with the corresponding intermediates. In any case, when we performed Curtin–Hammett simulations that eliminated the effect of these intermediates, we obtained a **2e(Sz)** : **2e(aS)** ratio of 84 : 16, which is virtually identical to the value obtained after numerical simulation.

Finally, the dehydration of dehydrolinalool (**1f**) was analyzed. The reaction profiles and the main geometrical features of the respective transition structures are shown in Fig. 9 and 10, respectively. In this reaction, there are three C–H bonds at the alpha position with respect to the OH group. Therefore, we analyzed the energetic profiles associated with the generation of two highly substituted (Saytzeff) alkenes **(*Z*)-2f(Sz)** and **(*Z*)-2f (Sz)** and one less substituted (anti-Saytzeff) alkene **2f(aS)**. As

Open Access Article. Published on 31 January 2024. Downloaded on 2/13/2026 9:36:17 AM. This article is licensed under a Creative Commons Attribution 3.0 Unported Licence.

expected, in all cases, the reaction is a stepwise elimination, in which a stable propargyl–tertiary carbocation intermediate is generated after the initial C–O bond cleavage. The computed activation barriers associated with the step are in the range of 27–29 kcal mol^{-1}, with small energy variations between the transition structures depending on the C–H···Cu interaction considered. As indicated above, those differences cannot be directly related to the final regioselectivity, since ionic pairs **INTf** and transition structures **TS2f**, associated with the H-elimination, play a significant role. As in the preceding case, we estimated the formation of alkenes **3f** in terms of the respective product complexes **PCf:**

$$\text{rate}(E\text{-Saytzeff}) = \frac{\text{d}[(E)\text{-PCf(Sz)}]}{\text{d}t} = k_2^{\text{Sz}}[(E)\text{-INTf(Sz)}] \quad (16)$$

$$\text{rate}(Z\text{-Saytzeff}) = \frac{\text{d}[(Z)\text{-PCf(Sz)}]}{\text{dt}} = k_2^{\text{Sz}}[(Z)\text{-INTf(Sz)}] \quad (17)$$

$$\text{rate}(\text{anti-Saytzeff}) = \frac{\text{d}[\text{PCf(aS)}]}{\text{d}t} = k_2^{\text{Sz}}[\text{INTf(aS)}] \quad (18)$$

The corresponding intermediate matrix Y_f includes the equilibrated reactive complexes **RCf** and the ionic intermediates **INTf:**

$$Y_f = \begin{pmatrix} [\text{RCf}] \\ [(E)\text{-INTf(Sz)}] \\ [(Z)\text{-INTf(Sz)}] \\ [\text{INTf(aS)}] \end{pmatrix} \quad (19)$$

Matrix K_f, which includes the kinetic constants indicated in Fig. 9, is as follows:

$$K_f = \begin{pmatrix} k_1^{E\text{-Sz}} + k_1^{Z\text{-Sz}} + k_1^{\text{aS}} & -k_{-1}^{E\text{-Sz}} & -k_{-1}^{Z\text{-Sz}} & -k_1^{\text{aS}} \\ -k_1^{E\text{-Sz}} & k_{-1}^{E\text{-Sz}} + k_2^{E\text{-Sz}} & 0 & 0 \\ -k_1^{Z\text{-Sz}} & 0 & k_{-1}^{Z\text{-Sz}} + k_2^{Z\text{-Sz}} & 0 \\ -k_1^{\text{aS}} & 0 & 0 & k_{-1}^{\text{aS}} + k_2^{\text{aS}} \end{pmatrix} \quad (20)$$

Following the above-described procedure and using eqn (16)–(20), we obtained the kinetic profile shown in Fig. 8B. According to our results, the calculated **(*E*)-2f(Sz) : (*Z*)-2f(Sz) : 2f (aS)** ratio is 51 : 28 : 21, which corresponds to a Saytzeff : anti-Saytzeff ratio of 79 : 21, which is in excellent agreement with the 80 : 20 ratio reported by Hoffman *et al.*[10] Also in this case, we did not find transition structures among **(*E*)-INf(Sz)**, **INTf (aS)** and **(*Z*)-INTf(Sz).** Following the same considerations indicated for the previous transformation, we tested the distribution of isomers applying the Curtin–Hammett kinetics and found a ratio of 68 : 18 : 14, which is in lower agreement with the experimental data (see Fig. 8B).[10]

4. Conclusions

In this work, we have presented a DFT study on the reaction mechanisms associated with the dehydration of alcohols catalyzed by $CuSO_4$. Our calculations show that the process corresponds to a concerted but asynchronous type II dyotropic reaction for primary alcohols, in which the C–O bond breaking event develops earlier than the C–H cleavage event. In the cyclic transition structure, the copper(II) atom plays a crucial role by assisting the hydroxyl moiety release. As far as secondary or tertiary alcohols are concerned, the reaction profile evolves towards a stepwise mechanism in which the initial C–O bond breaking process generates a carbenium–hydroxyl ionic pair intermediate, which gives rise to the final alkene through an H-abstraction step assisted by an oxygen atom of the sulfate moiety. Analyses of the energy profiles show that the activation barrier associated with the first step is the highest one, but the second transition structure lays above in energy and plays a significant role in the selectivity of the process through which different products can be obtained. This complex kinetic situation can be analyzed within a Curtin–Hammett framework. However, numerical integration of the respective ensembles of differential equations provides computed selectivities corresponding to the dehydration reactions of 2-methyl-2-hexanol (**1e**) and dehydrolinalool (**1f**) that agree reasonably well with the experimental reports. The computed reactivity trend for the dehydration of alcohols following the proposed mechanisms is tertiary > secondary > primary, which is in perfect agreement with the experimental results. Therefore, in general, anti-Saytzeff alkenes will be obtained as major dehydration products. This situation poses an important challenge for the regioselective synthesis of anti-Saytzeff alkenes of interest in the fragrance industry, such as the precursor of Galbascone (Dynascone).

Author contributions

J. S.-Q.: conceptualization, funding acquisition, project administration, supervision, and validation. C. L.-C.: conceptualization, project administration, supervision, and validation. A. de C.: data curation, formal analysis, investigation, methodology, validation, visualization, writing – original draft, and software. A. A. and I. A.: data curation, formal analysis, investigation, methodology, and validation. F. P. C: conceptualization, funding acquisition, project administration, supervision, formal analysis, methodology, validation, resources, and writing – review & editing. All the authors revised and contributed to the final version of the manuscript.

Conflicts of interest

The authors declare that they have no known competing financial interests that could have influenced the work reported in this article.

Acknowledgements

Financial support for this work was provided by the Spanish Ministerio de Ciencia, Innovación y Universidades (MICIN/AEI/PID2019-104772GB-I00 and MCIN/AEI/RED2022-134287-T) and

 This journal is © The Royal Society of Chemistry 2024

Open Access Article. Published on 31 January 2024. Downloaded on 2/13/2026 9:36:17 AM. This article is licensed under a Creative Commons Attribution 3.0 Unported Licence.

the Gobierno Vasco/Eusko Jaurlaritza (GV/EJ, Grant IT-1553-22). The authors thank SGI/IZO-SGIker of the UPV/EHU and the DIPC for the generous allocation of computational resources.

References

1 W. H. Brown, C. S. Foote, B. L. Iverson, E. V. Anslyn and B. M. Novak, *Aldehydes and Ketones. Organic Chemistry*, Brooks/Cole Belmont, CA, 2012.
2 M. B. Smith and A. J. March, *March's Advanced Organic Chemistry: Reactions, Mechanisms and Structure*, Wiley Interscience, New York, 2007.
3 E. V. Anslyn and D. A. Dougherty, *Modern Physical Organic Chemistry*, University Science Books, Sausalito, CA, 2005.
4 M. T. Reetz, *Angew. Chem., Int. Ed. Engl.*, 1972, **11**, 129–130.
5 M. T. Reetz, *Tetrahedron*, 1973, **29**, 2189–2194.
6 M. T. Reetz, in *Advances in Organometallic Chemistry*, ed. F. G. A. Stone and R. West, Academic Press, 1977, vol. 16, pp. 33–65.
7 I. Fernández, F. P. Cossío and M. A. Sierra, *Chem. Rev.*, 2009, **109**, 6687–6711.
8 F. C. Whitmore and E. Rohrmann, *J. Am. Chem. Soc.*, 1941, **63**, 2033–2035.
9 G. W. Francis and J. F. Berg, *Acta Chem. Scand., Ser. B*, 1977, **31**, 721–722.
10 R. V. Hoffman, R. D. Bishop, P. M. Fitch and R. Hardenstein, *J. Org. Chem.*, 1980, **45**, 917–919.
11 T. Pieterse, C. Marais and B. C. B. Bezuidenhoudt, *ARKIVOC*, 2022, **2022**, 217–231.
12 E. J. Eisenbraun, K. W. Payne and J. S. Bymaster, *Org. Prep. Proced. Int.*, 2006, **32**, 557–561.
13 T. Nishiguchi, N. Machida and E. Yamamoto, *Tetrahedron Lett.*, 1987, **28**, 4565–4568.
14 T. Nishiguchi and C. Kamio, *J. Chem. Soc., Perkin Trans. 1*, 1989, 707–710, DOI: **10.1039/P19890000707**.
15 I. Fernández, F. M. Bickelhaupt and F. P. Cossío, *Chem. – Eur. J.*, 2012, **18**, 12395–12403.
16 I. Fernández, F. P. Cossío and M. A. Sierra, *Acc. Chem. Res.*, 2011, **44**, 479–490.
17 I. Fernández and F. P. Cossío, *J. Comput. Chem.*, 2016, **37**, 1265–1273.
18 F. Cervantes-Navarro, A. de Cózar, F. P. Cossío, M. A. Fernández-Herrera, G. Merino and I. Fernández, *Chem. Commun.*, 2015, **51**, 5302–5305.
19 G. Frenking, F. P. Cossío, M. A. Sierra and I. Fernández, *Eur. J. Org. Chem.*, 2007, **2007**, 5410–5415.
20 I. Fernández, M. A. Sierra and F. P. Cossío, *J. Org. Chem.*, 2007, **72**, 1488–1491.
21 I. Fernández, M. A. Sierra and F. P. Cossío, *Chem. – Eur. J.*, 2006, **12**, 6323–6330.
22 M. A. Sierra, I. Fernández, M. J. Mancheño, M. Gómez-Gallego, M. R. Torres, F. P. Cossío, A. Arrieta, B. Lecea, A. Poveda and J. Jiménez-Barbero, *J. Am. Chem. Soc.*, 2003, **125**, 9572–9573.
23 Y. Zhao and D. G. Truhlar, *Acc. Chem. Res.*, 2008, **41**, 157–167.
24 Y. Zhao and D. G. Truhlar, *J. Chem. Phys.*, 2006, **125**, 194101.
25 J. Tao, J. P. Perdew, V. N. Staroverov and G. E. Scuseria, *Phys. Rev. Lett.*, 2003, **91**, 146401.
26 J. P. Perdew, A. Ruzsinszky, G. I. Csonka, L. A. Constantin and J. Sun, *Phys. Rev. Lett.*, 2009, **103**, 026403.
27 S. Grimme, S. Ehrlich and L. Goerigk, *J. Comput. Chem.*, 2011, **32**, 1456–1465.
28 M. J. Frisch, *et al.*, *Gaussian 16, Revision C.01*, Gaussian, Inc, Wallingford, CT, 2016.
29 J. Tomasi, B. Mennucci and R. Cammi, *Chem. Rev.*, 2005, **105**, 2999–3094.
30 P. J. Hay and W. R. Wadt, *J. Chem. Phys.*, 1985, **82**, 270–283.
31 R. G. Parr and W. Yang, *Density Functional Theory of Atoms and Molecules*, Oxford University Press, Oxford, New York, 1989.
32 J. W. McIver Jr. and A. Komornicki, *J. Am. Chem. Soc.*, 1972, **94**, 2625–2633.
33 K. Fukui, *Acc. Chem. Res.*, 1981, **14**, 363–368.
34 H. P. Hratchian and H. B. Schlegel, in *Theory and Applications of Computational Chemistry: The First 40 Years*, ed. E. Dykstra, G. Frenking, K. S. Kim and G. Scuseria, Elsevier, Amsterdam, 2005, pp. 195–249.
35 F. Weinhold and C. R. Landis, *Valency and Bonding –A Natural Bond Orbital Donor-Acceptor Perspective*, Cambridge University Press, Cambridge CB2 2RU, UK, 2005.
36 K. B. Wiberg, *Tetrahedron*, 1968, **24**, 1083–1096.
37 M. Agirre, S. Henrion, I. Rivilla, J. I. Miranda, F. P. Cossío, B. Carboni, J. M. Villalgordo and F. Carreaux, *J. Org. Chem.*, 2018, **83**, 14861–14881.
38 A. Moyano, M. A. Pericas and E. Valenti, *J. Org. Chem.*, 1989, **54**, 573–582.
39 J. I. Seeman, *J. Chem. Educ.*, 1986, **63**, 42.
40 J. I. Seeman, *Chem. Rev.*, 1983, **83**, 83–134.
41 B. K. Carpenter, *Determination of Organic Reaction Mechanisms*, JohnWiley & Sons, New York, 1984.
42 J. Lin, D.-W. Guo and Y.-Q. Tian, *Cryst. Growth Des.*, 2008, **8**, 4571–4575.
43 A. Lapczynski, S. P. Bhatia, C. S. Letizia and A. M. Api, *Food Chem. Toxicol.*, 2008, **46**, S117–S120.
44 J. Scognamiglio, C. S. Letizia and A. M. Api, *Food Chem. Toxicol.*, 2013, **62**, S74–S82.
45 D. Fan, D.-J. Dai and H.-S. Wu, *Materials*, 2013, **6**, 101–115.